Journal of Power Sources 195 (2010) 3513–3522

Contents lists available at ScienceDirect

Journal of Power Sources

journal homepage: www.elsevier.com/locate/jpowsour

Residual stress and plastic strain analysis in the brazed joint of bonded compliant seal design in planar solid oxide fuel cell

Wenchun Jiang[a,*], S.T. Tu[b], G.C. Li[a], J.M. Gong[c]

[a] College of Mechanical and Electronic Engineering, China University of Petroleum, Dongying 257061, PR China
[b] Key Laboratory of Safety Science of Pressurized System, Ministry of Education, East China University of Science and Technology, Shanghai 200237, PR China
[c] School of Mechanical and Power Engineering, Nanjing University of Technology, Nanjing 210009, PR China

ARTICLE INFO

Article history:
Received 28 November 2009
Received in revised form
16 December 2009
Accepted 16 December 2009
Available online 22 December 2009

Keywords:
Solid oxide fuel cell
Bonded compliant seal (BCS)
Residual stress
Finite element method

ABSTRACT

This paper uses finite element method (FEM) to predict the residual stress and plastic strain in the brazed joint of sealing foil-to-window frame in bonded compliant seal (BCS) design in a planar solid oxide fuel cell (PSOFC). The effects of window frame material type, sealing foil thickness, filler metal thickness and window frame thickness on residual stress and plastic strain are discussed. Large residual stress is generated in the joint, and the stress and strain are concentrated around the fillet. It is proved that the BCS design can mitigate and trap some residual stress by plastic deformation within the sealing foil. The residual stress and the ability of trapping stress of sealing foil are affected by window frame material and structure thickness. Based on the comprehensive considerations of the impact of residual stress and plastic strain, Alloy 625 as a window frame material is found to be better than Haynes 214, Hastelloy X and SUS 316L. The optimum thickness of sealing foil and filler metal BNi2 are found to be 150 μm and 75 μm, respectively. The residual stress and plastic strain are increased with the increase of window frame thickness.

1. Introduction

Planar solid oxide fuel cell (PSOFC) is a technology which converts chemical energy into electrical energy [1,2]. Its advantages are high efficiency in energy utilization [3], compact structure [4], pollution-free [5], etc. Therefore, it is widely used in distributed power, fixed station, mobile power, transportation and military [6,7]. The PSOFC operates at hostile environment: (1) a high operating temperature of 750 °C and (2) continuous service at an oxidizing atmosphere at cathode side and a wet reducing gas at anode side. The harsh conditions put forward a higher requirement for sealing technology, aiming to ensure the structure integrity and an anticipated lifetime of 10,000 h. The leakage, which is generated from manufacture defects or structure degradation in service, can cause a serious decline in system performance, power generation and fuel utilization efficiency. Therefore, the hermeticity in PSOFC is very important.

In order to ensure the safe operation of PSOFC, considerable effort has been paid on the sealants in recent years [8–11]. There are two types of cell-to-frame seals used in window frame PSOFC: rigid bonded glass seal and compressive gasket seal. Their advantages and disadvantages have been described in Ref. [8]. In recent, a third sealing method named the bonded compliant seal (BCS) has been developed by Weil et al. [12,13], which incorporates the advantages of both rigid and compressive sealing. In BCS design, a thin metal foil is bonded to the adjacent metal and ceramic components, which can mitigate and trap some thermal stress as elastic or plastic strain within the sealing foil. It has been proved that the BCS structure presents good strength in as-brazed and thermally cycled conditions [12]. Weil and Koeppel [14] found that the BCS design offered obvious advantages over glass-ceramic and braze sealing based on thermal stress considerations. Jiang and Chen [15] also performed thermal stress analysis to an operating PSOFC with BCS design by finite element method (FEM), and the effects of temperature non-uniformity and cell voltage on thermal stress were also discussed.

In BCS design, an important problem is the joining between sealing foil and window frame, because it belongs to dissimilar joining. The residual stress generated by dissimilar welding [16–18] will have a great effect on creep [19], stress corrosion cracking [20,21] and fatigue [22,23]. Another, BNi2 used as filler metal, contains melting point depressants such as boron and silicon [24]. However, the boron and silicon will generate some brittle compounds, thereby reducing the structural strength [25,26]. With regard to the residual stress studies of PSOFC, the main attention was paid on the electrolyte layer [27–29]. Little attention has been paid to the joint

* Corresponding author. Tel.: +86 546 8391776; fax: +86 546 8393620.
E-mail address: jiangwenchun@upc.edu.cn (W. Jiang).

0378-7753/$ – see front matter © 2009 Elsevier B.V. All rights reserved.
doi:10.1016/j.jpowsour.2009.12.066

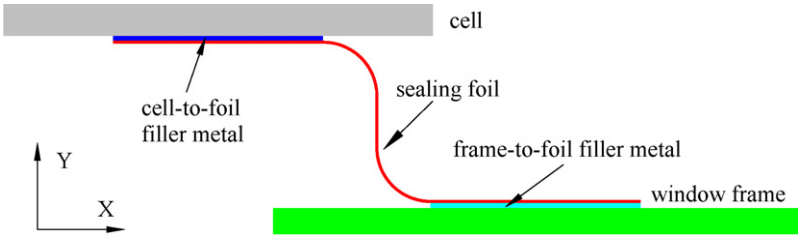

Fig. 1. The cross-section of the BCS structure.

Table 1
Dimensions and materials for the components of BCS structure.

Component	Cell	Cell-to-foil braze	Foil	Foil-to-frame braze	Frame
Thickness (μm)	600	100	50	100	500
Material	Ni–YSZ/YSZ	Ag–4 mol% CuO	FeCrAlY	BNi-2	Haynes 214

between sealing foil and window frame. Therefore, the as-brazed residual stress in BCS design is studied by FEM in this paper.

2. Finite element model

2.1. Geometrical model and meshing

Fig. 1 shows the cross-section of the BCS structure. An S-shaped sealing foil is brazed to the cell and window frame by silver-based filler metal (Ag–4%CuO) and BNi2 filler metal, respectively. The thickness of each component is listed in Table 1, which is the same as Ref. [13]. Finite element code ABAQUS is used to simulate the residual stress. A 2D plane strain finite element model is built and the meshing of the local is shown in Fig. 2. In total, 2793 nodes and 2452 elements are meshed.

2.2. Material properties

The materials of the components in the BCS structure are listed in Table 1, which is also the same as Ref. [13]. For the residual stress analysis, temperature-dependent mechanical properties of materials are incorporated. The material properties relevant to residual stress are elastic modulus, yield stress, Poisson's ratio, and the coefficient of thermal expansion (CTE). In fact, the cell in the planar stacks is a composite structure composed of anode, electrolyte layer and cathode layer. However, in the present study, the attention is focused on the joint of sealing foil-to-window frame, and therefore the material of the cell is assumed to be the same as anode material (Ni-YSZ). The temperature-dependent mechanical properties of these materials are obtained from Refs. [14,30] and have not been listed here to decrease the paper length.

In this paper, Haynes 214 and FeCrAlY are used as the materials of window frame and sealing foil, respectively. This is because the both contain Al in high enough concentration (>3%) and present a good oxidation resistance performance. In BCS design, this property is very important because the material should be as thin as possible to concentrate mismatch and residual stresses way from the adjoining substrates, yet still present low metal loss at high-temperature oxidizing conditions so that the strength and long-term durability are retained [12].

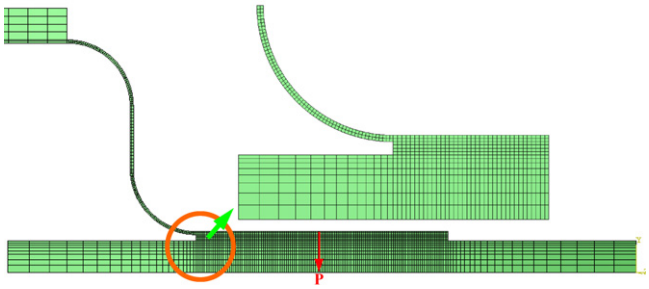

Fig. 2. Finite element meshing.

2.3. Residual stress analysis

The BCS structure is fabricated by brazing. The stacking is heated to the brazing temperature of 1050 °C and then cooled to ambient temperature. At the high temperature, the structure is at stress-free state. Therefore, the as-brazed residual stress in sealing foil-to-frame joint is simulated during the cooling from 1050 °C to 20 °C.

For the present used materials, solid-state phase transformation does not occur. Therefore, the total strain rate can be decomposed into three components as follows:

$$\dot{\varepsilon} = \dot{\varepsilon}^{e} + \dot{\varepsilon}^{p} + \dot{\varepsilon}^{ts} \quad (1)$$

where $\dot{\varepsilon}^{e}$, $\dot{\varepsilon}^{p}$ and $\dot{\varepsilon}^{ts}$ stands for elastic strain, plastic strain and thermal strain, respectively. Elastic strain is modeled using the isotropic Hooke's law with temperature-dependent Young's modulus and Poisson's ratio. The thermal strain is calculated using the temperature-dependent CTE. For the plastic strain, a rate-independent plastic model is employed with Von Mises yield surface, temperature-dependent mechanical properties and linear kinematic hardening model.

This analysis was simplified according to the following considerations: (1) the capillarity of filler metal at brazing temperature is out of view; (2) the solutionizing and the diffusion of the filler components to base metal are not included; (3) the creep behavior during the brazing process is not considered; (4) the fluid flow of the filler at brazing temperature is not simulated.

3. Results and discussion

3.1. Residual stress distribution

Residual stress components from FE analysis are obtained in the following direction: (1) longitudinal stress S11, represents the stress in *X*-axis direction; (2) transverse stress S22, refers the stress in *Y*-axis direction; (3) shear stress S12, is the stress in the *XY*-plane.

Fig. 3 shows the contours of S11, S22 and S12 distribution. It can be seen that their peak values are 727 MPa, 165 MPa and 166 MPa, respectively, which are all located at the fillet. The stress concentration at the fillet is caused by three reasons: one reason is the structure discontinuity around the fillet, which can cause stress

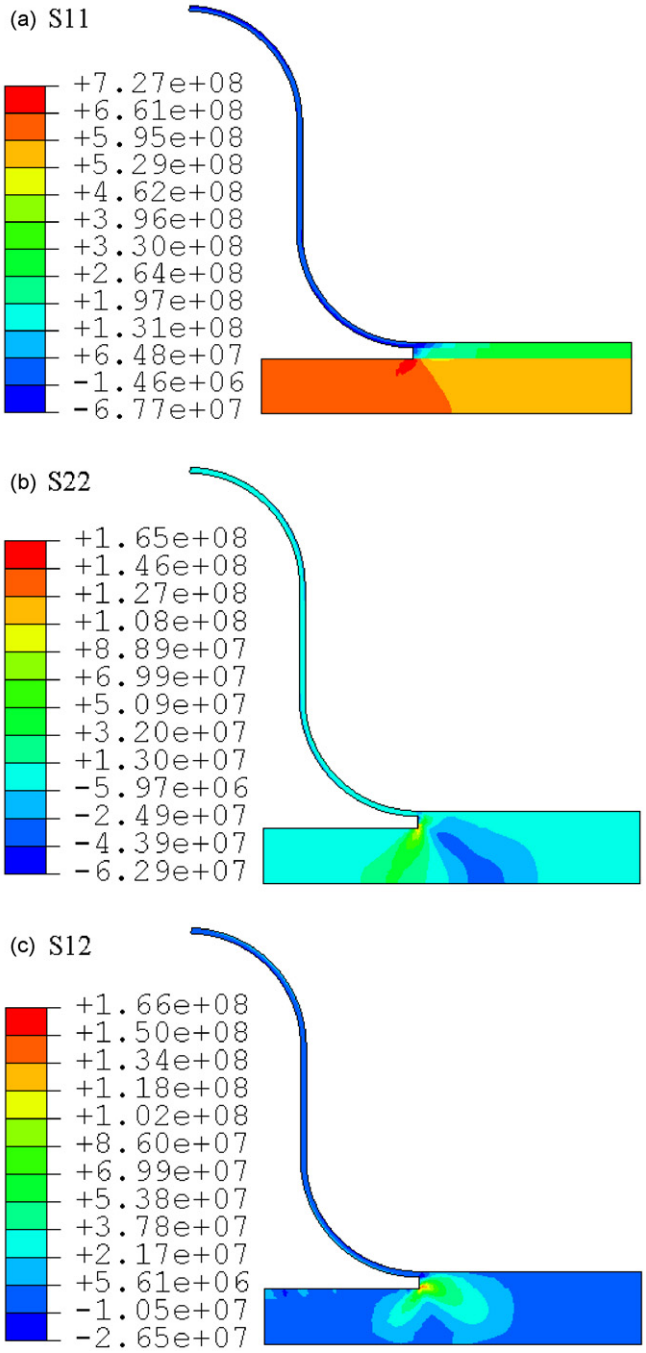

Fig. 3. Residual stress contours: (a) S11; (b) S22; (c) S12.

concentration easily. The second reason is the mechanical properties mismatch among the sealing foil, filler metal BNi2, and window frame. Another, during the brazing, the parts dislocation in the stacking is forbidden because that the dislocation can cause flaws. So the stacking is clamped tightly to avoid mismatch, which leads to the generation of restraint stress.

Fig. 4 shows the residual stress distribution along path P shown in Fig. 2. It shows that S22 and S12 are about zero. The reason is that the total thickness of foil, filler metal and window frame is very thin, and therefore the S22 is very small. But in the longitudinal direction, the thickness is relatively thick and therefore S11 is large. S11 in the sealing foil and BNi2 filler metal is 264 MPa and 270 MPa, respectively, while it is 554 MPa in the window frame. The yield strength of window frame is larger that those of sealing foil and

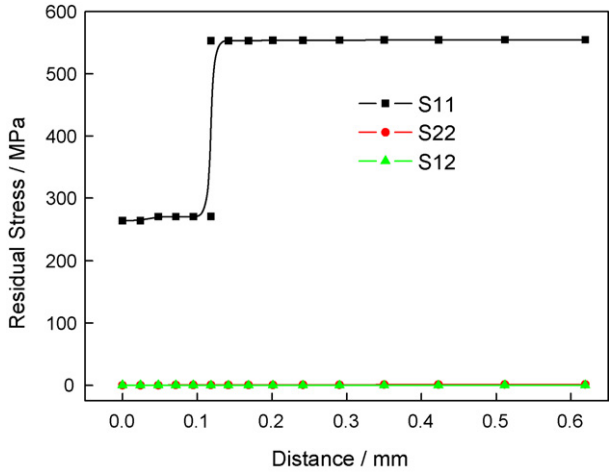

Fig. 4. Residual stress distribution along path P.

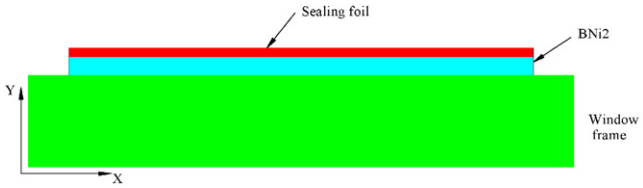

Fig. 5. Finite element model without S-shaped foil.

BNi2, so the S11 in window frame is larger than sealing foil and BNi2. The stresses in sealing foil and BNi2 are nearly the equal for almost the same yield strength.

Haynes 214 and FeCrAl both will form alumina upon oxidation. Alumina has a much lower CTE and very high stiffness than the metal substrates. As a result, high residual stress will be generated in the thin oxide layer. But this residual stress and its effect have not been researched in this paper, which should be explored in depth in the future.

3.2. Verification for the function of S-shaped sealing foil

In the BCS design as shown in Fig. 1, the innovation is the application of an S-shaped sealing foil. The sealing foil can mitigate and trap some thermal stresses in the operating condition, which has not been verified in Refs. [12–15]. This function is verified in this

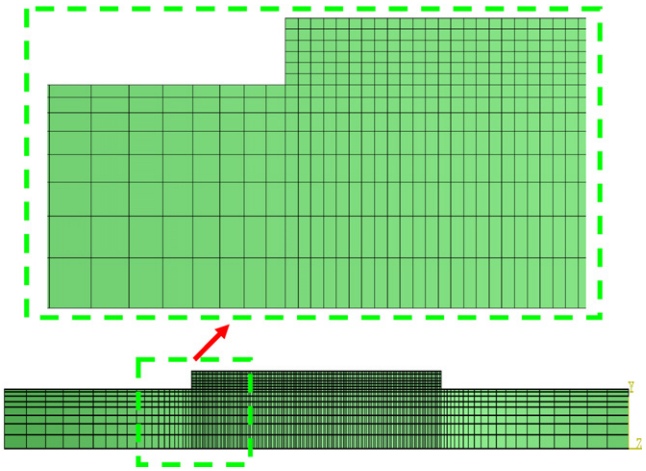

Fig. 6. Finite element meshing without S-shaped foil.

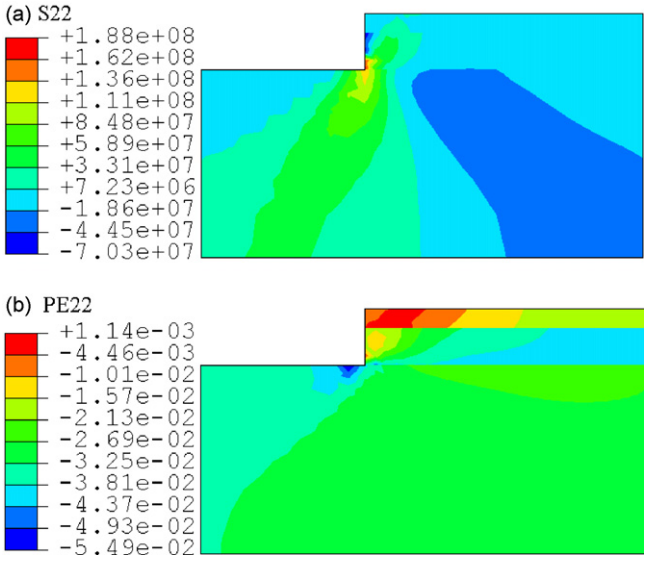

Fig. 7. The stress (a) and plastic strain (b) without S-shaped sealing foil.

section. A new finite element model without S-shaped foil is built, as shown in Fig. 5. And its finite element meshing is displayed in Fig. 6. The thin foil plate is brazed to window frame by BNi2 filler metal. Their dimensions and materials are the same as those in Table 1. The results show that the stresses are still concentrated in the fillet. The stress and strain in *Y*-direction have great effect on crack initiation and propagation. So the discussion here is paid on the stress and strain in *Y*-direction.

Fig. 7 shows the stress and plastic strain (PE22) along *Y*-direction. The maximum of S22 is 188 MPa, which is larger than that with S-shaped foil. The maximum of plastic strain is 0.114%, which is located at the ends of the interface between sealing foil and BNi2. Fig. 8 shows the plastic strain with S-shaped sealing foil. It can be seen that the maximum of plastic strain is 0.0874%. With the application of S-shaped foil, the maximum plastic strain has been decreased about 24%. This means that some stresses and strain have been trapped by the S-shaped sealing foil. The S-shaped sealing foil is similar to an elastic spring. As shown in Fig. 8, the maximum plastic strain is located at the ends of the interface between sealing foil and BNi2 around the fillet. But some brittle phases would be generated around the interface when BNi2 is used [31], which could be the initiation of cracks. The lower the interface strain, the better the

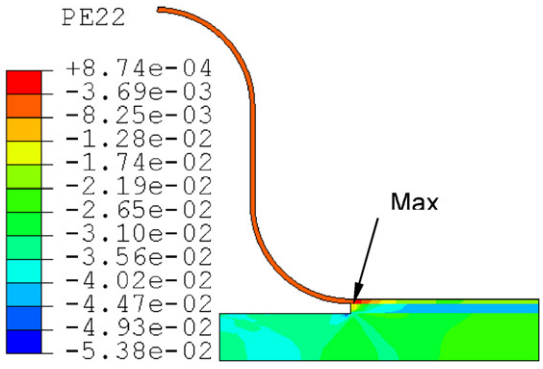

Fig. 8. Plastic strain with S-shaped sealing foil.

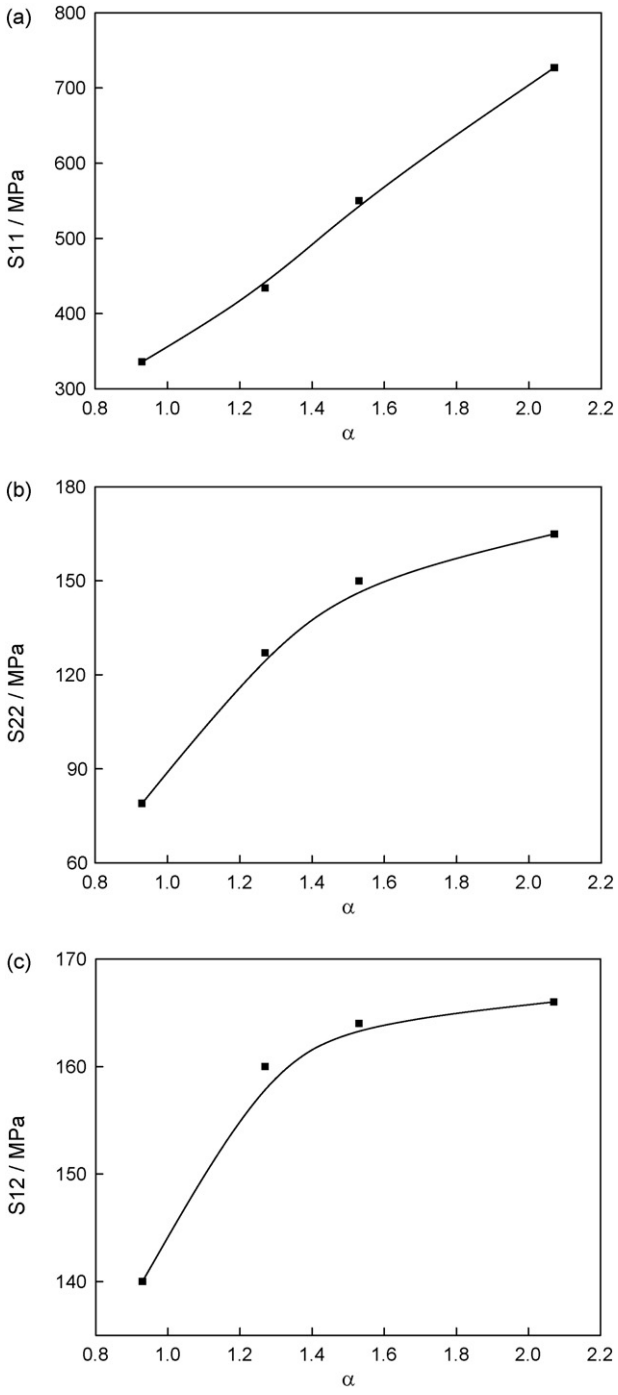

Fig. 9. Effect of α on the peak values: (a) S11; (b) S22; (c) S12.

Table 2
The mechanical properties for window frame.

Material	Haynes 214	Alloy 625	Hastelloy X	SUS 316L	BNi2
CTE (μm/(m°C))	13.3	12.8	15.0	15.2	13.4
Yield strength (MPa)	620	460	380	278	300
α	2.07	1.53	1.27	0.93	–
β	0.99	0.96	1.12	1.13	–

joint strength. Therefore, the role of S-shaped sealing foil is obvious. It is hoped that more stresses and strain could be absorbed by the sealing foil.

Although large residual stresses are generated in the fillet as shown in Fig. 3, they could be relaxed due to creep at high temperature. The plastic strain in the fillet would be very large [19] if there were no S-shaped sealing foil. But with the application of S-shaped foil, some creep strain can be trapped by the foil, and the stress and strain concentration in the fillet can be decreased, through which the cracks could be avoided.

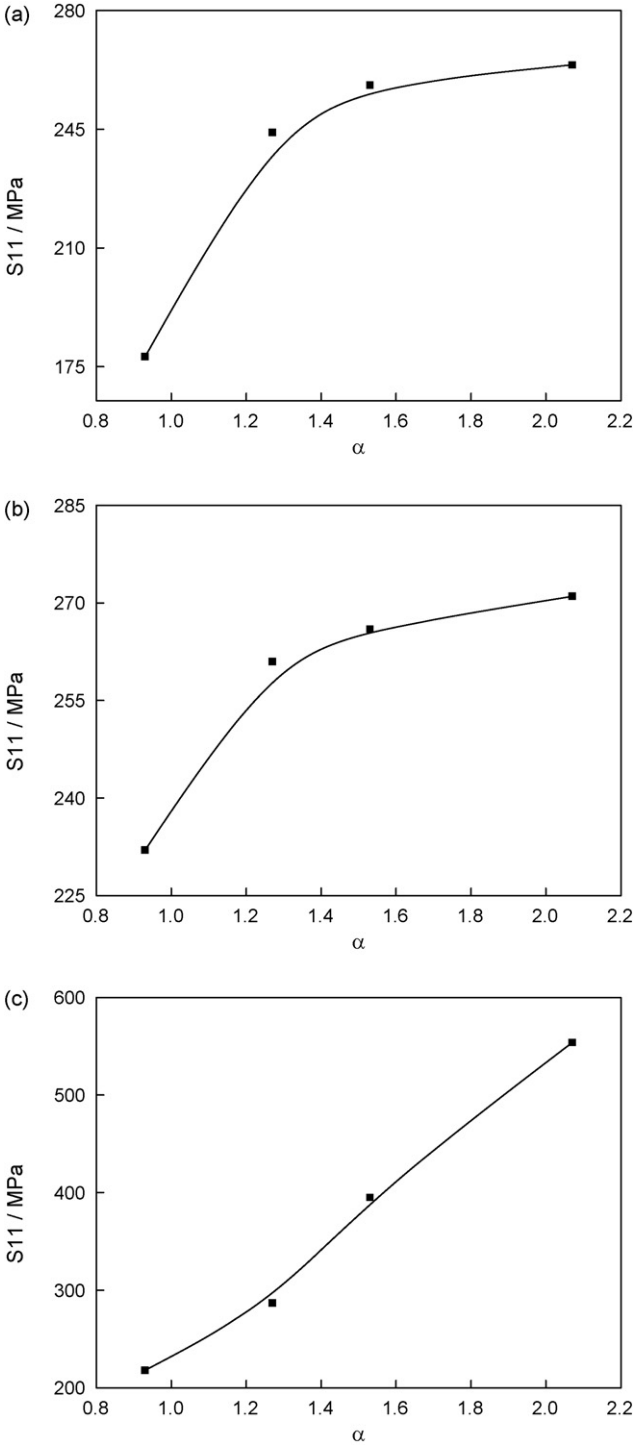

Fig. 10. Effect of α on S11 in sealing foil (a), BNi2 (b) and window frame (c).

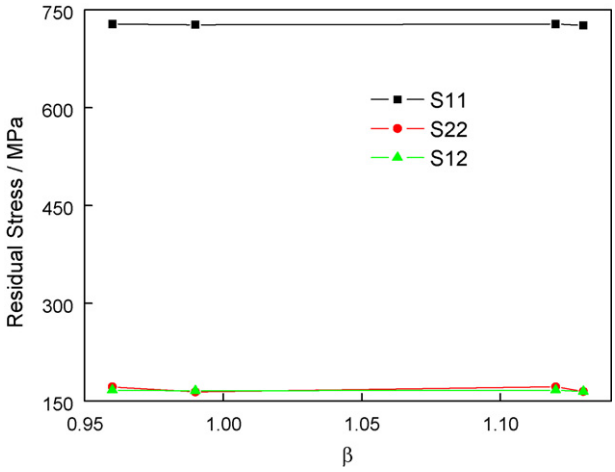

Fig. 11. Effect of β on peak residual stresses.

The peak value level of PE22 represents the ability to absorb plastic stain for S-shaped sealing foil. But the ability is affected by many factors, such as material properties of window frame, the sealing foil thickness, filler metal thickness, window frame thickness, etc. Therefore, the effects of material and geometric parameters on residual stress and plastic strain were discussed in the following sections.

4. Effect of material type of window frame on residual stress

The window frame material of BCS structure in Ref. [14] is Haynes 214. Haynes 214 was used because it is a type of alumina scale-forming alloy and good creep-resistance strength. But its yield strength is up to 620 MPa, which is far larger than those of sealing foil and BNi2. The mismatching of mechanical properties can cause large residual stresses. In this section, the effect of material type for window frame on residual stress and plastic strain is discussed. Hastelloy X, Inconel Alloy 625 and SUS 316L are all good creep-resistance materials, which are used as the material of window frame in this section. Their yield strength and CTE at room temperature are listed in Table 2. The yield strength mismatch coefficient α and CTE mismatch coefficient β are calculated, respectively, by

$$\alpha = \frac{\sigma_F}{\sigma_W} \quad (2)$$

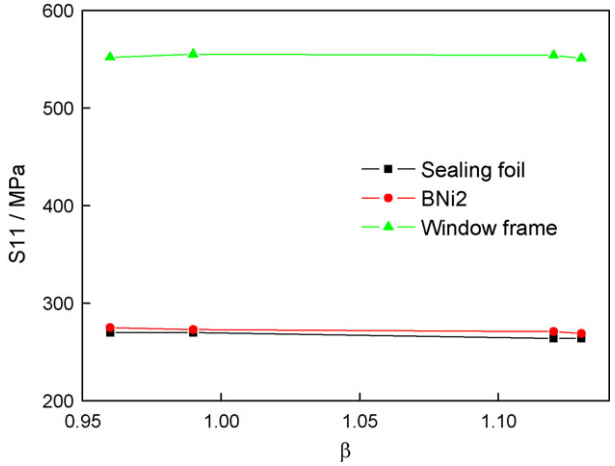

Fig. 12. Effect of β on S11 in sealing foil, BNi2 and window frame.

$$\beta = \frac{C_F}{C_W} \quad (3)$$

where σ_F and σ_W standard for the yield strength of window frame and filler metal BNi2, respectively. C_F and C_W are the CTE of window frame and filler metal BNi2, respectively. The values of α and β are listed in Table 2.

Keeping the rest parameters constant, another three FE models with different window frame material were calculated and compared. It is found that when the frame material is changed, the stress distribution law does not change. But the stress values are different. Fig. 9 shows the effect of α on the peak stresses in the fillet. It can be seen that the peak values are increased as α increase. The peak values of S11 obtained by Haynes 214, Hastelloy X, Alloy 625 and SUS 316L are 727 MPa, 550 MPa, 434 MPa and 336 MPa, respectively. The corresponding maximum values of S22 are 165 MPa, 150 MPa, 127 MPa and 79 MPa, respectively. And the corresponding S12 obtained from them are 166 MPa, 164 MPa, 160 MPa and 140 MPa. When α is increased from 0.93 to 2.07, the peak values of S11, S22 and S12 are increased about 116%, 108% and 19%.

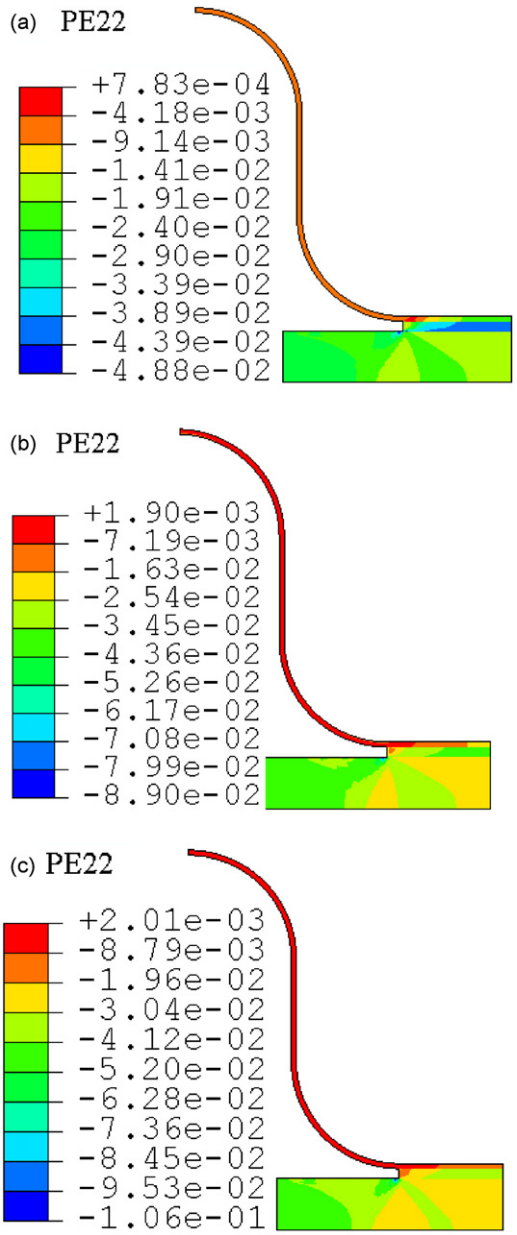

Fig. 13. Plastic strain PE22 obtained by Alloy 625 (a), Hastelloy X (b) and SUS 316L(c).

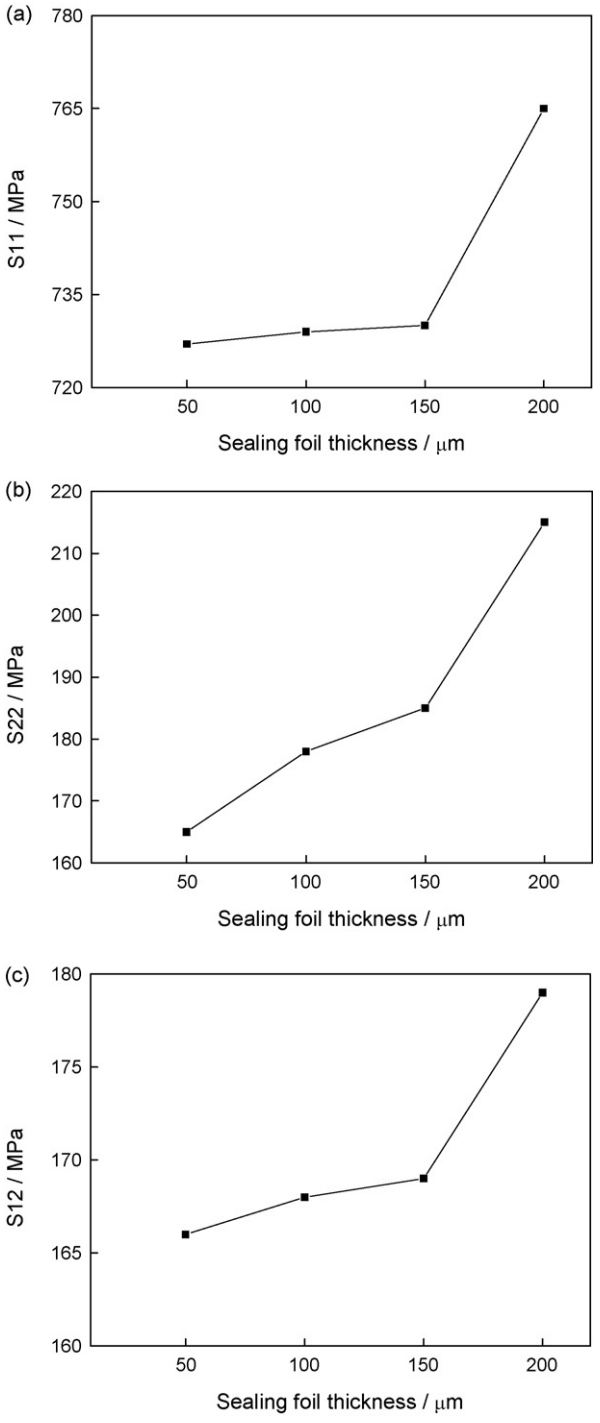

Fig. 14. Effect of sealing foil thickness on peak stresses: (a) S11; (b) S22: (c) S12.

Fig. 10 shows the effect of α on S11 in the sealing foil, BNi2 and window frame. It displays that the stresses in the three layers are also increased as α increase. S11 in sealing foil obtained by Haynes 214, Hastelloy X, Alloy 625 and SUS 316L are 264 MPa, 258 MPa, 244 MPa and 178 MPa, respectively. In BNi2 filler metal, the corresponding S11 are 271 MPa, 266 MPa, 261 MPa and 232 MPa. And S11 in window frame is 554 MPa, 395 MPa, 287 MPa and 218 MPa, respectively. When α is increased from 0.93 to 2.07, S11 in sealing foil, BNi2 and frame is increased about 48%, 17% and 154%.

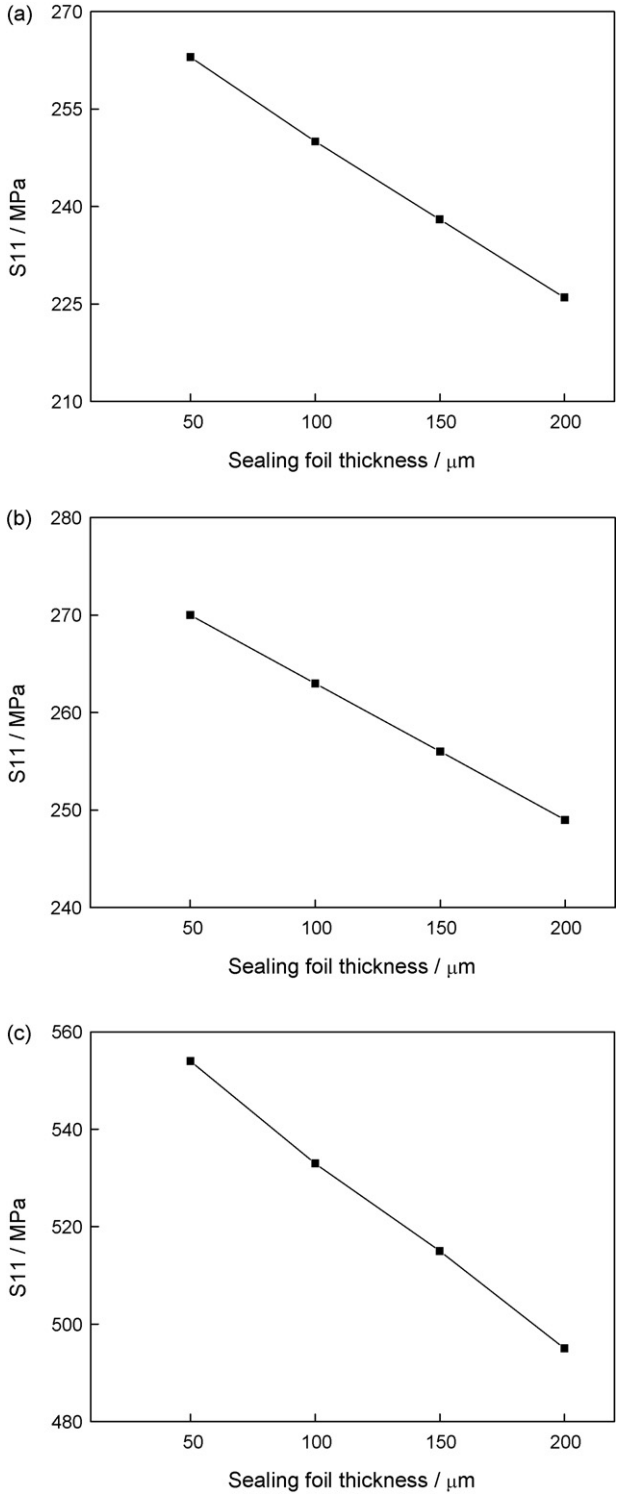

Fig. 15. Effect of sealing foil thickness on S11 in sealing foil (a), BNi2 (b) and Window frame (c).

Table 2 shows that the CTE of the selected four materials is different. One may ask whether the CTE has effect on residual stress. The contribution of CTE on residual stress is discussed here. It is assumed that the yield strengths of Hastelloy X, Alloy 625 and SUS316L are the same as that of Haynes 214. The effect of β on peak stresses is shown in Fig. 11, and Fig. 12 shows its effect on residual stress in sealing foil, BNi2 and window frame. It can be seen that the CTE has little effect on residual

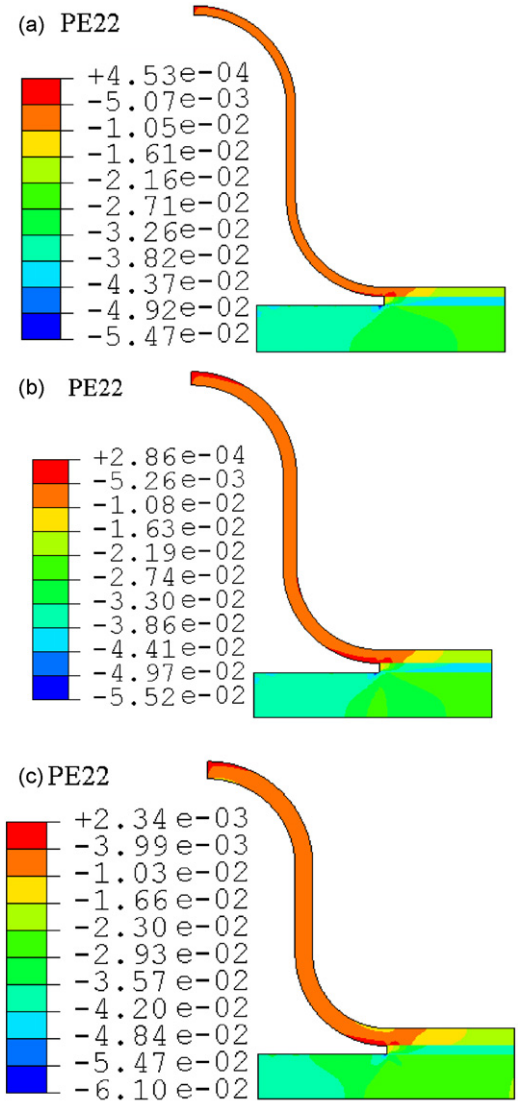

Fig. 16. The plastic strain with the different thickness of sealing foil: (a) 100 μm; (b) 150 μm; (c) 200 μm.

stress. The residual stress is mainly influenced by yield strength mismatch.

Fig. 13 shows PE22 obtained by Alloy 625, Hastelloy X and SUS 316L. Compared to Haynes 214 shown in Fig. 8, the maximum values are all located at the ends of interface between sealing foil and BNi2 around the fillet. The PE22 contour obtained by Alloy 625 shown in Fig. 13(a) displays that the peak value is 0.0783%, which is slightly smaller than that of Haynes 214. But the peak values obtained by Hastelloy X and SUS316L are increased to 0.19% and 0.201%, respectively. That is to say, the material type of window frame affects the ability to trap strain for sealing foil. Based on this, Haynes 214 and Alloy 625 materials are better than Hastelloy X and SUS316L. But the residual stresses obtained by Alloy 625 are smaller that those of Haynes 214.

5. Effect of thickness on residual stress

5.1. Effect of sealing foil thickness

Keeping the rest parameters constant, the thickness of sealing foil was changed to discuss its effect. Another three FE models

with a sealing foil thickness of 100 μm, 150 μm and 200 μm were developed and calculated. It was found the peak stresses are increased slightly as the sealing foil thickness increases from 50 μm to 150 μm, but it has a sudden increase when the thickness is 200 μm, as shown in Fig. 14. But S11 in sealing foil, BNi2 and window frame are decreased with the sealing foil thickness increase, as shown in Fig. 15. Although the sealing foil is with a function of spring, it also has stiffness. When the thickness of sealing foil is increased, its stiffness is also increased concurrently, and the sealing foil also has constraint against the fillet, which lead to the increase of peak stresses. When the thickness is increased to 200 μm, the stiffness and the constraint are big enough to cause a sudden stress increase. The PE22 distribution contours of the three models are shown in Fig. 16. Compared to Fig. 8, it can be seen that the maximum PE22 is decreased from 0.0874% to 0.0286% when the thickness is increased from 50 μm to 150 μm. But PE22 jumps to 0.234% when the sealing foil is 200 μm. Based on this, it can be concluded that the sealing foil should be determined around 150 μm.

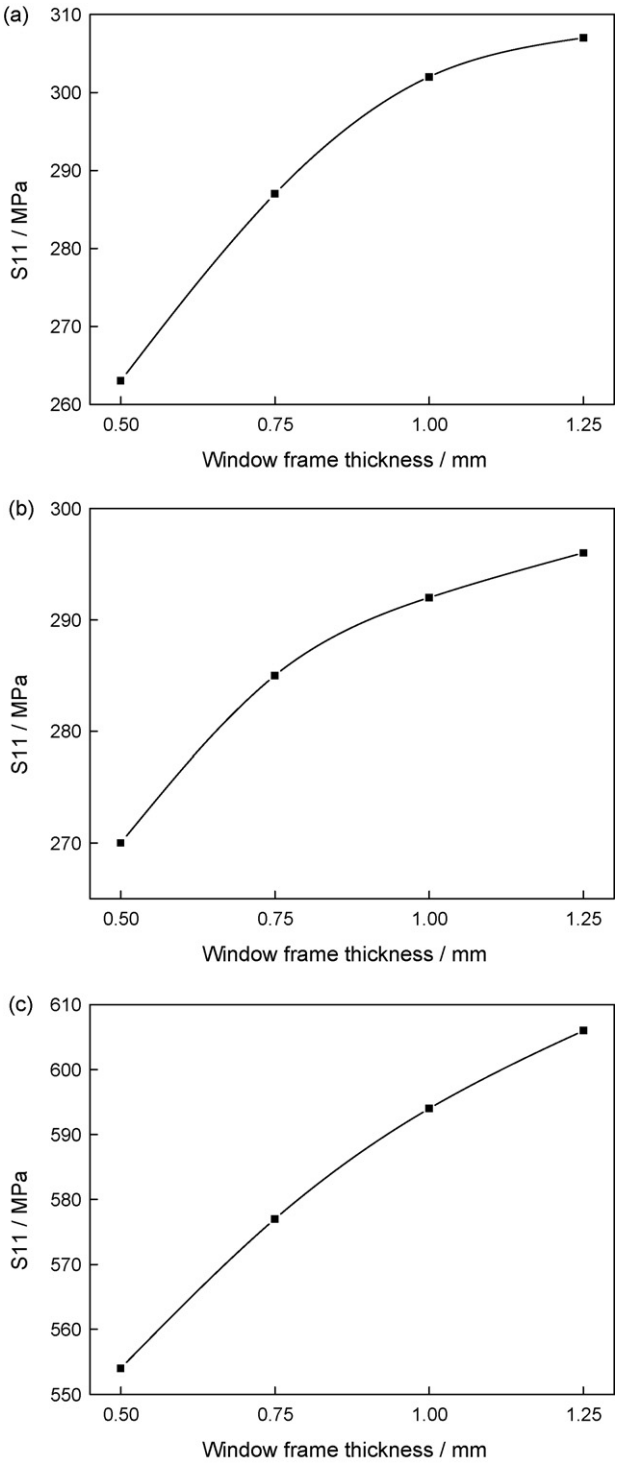

Fig. 17. Effect of window frame thickness on S11 in sealing foil (a), BNi2 (b) and window frame (c).

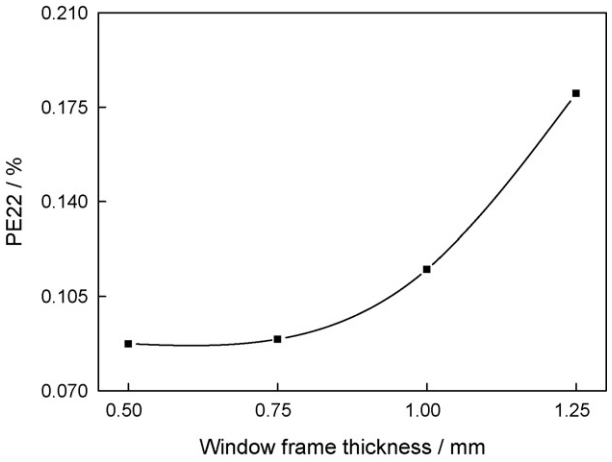

Fig. 18. Effect of window frame thickness on plastic strain.

5.2. Effect of window frame thickness

Keeping the rest parameters constant, another three FE models with a window frame thickness of 0.75 mm, 1 mm and 1.25 mm were developed and calculated. It was found the peak stresses are increased with the window frame thickness increase, which is not shown here to decrease the paper length. The effect of window frame thickness on S11 in sealing foil, BNi2 and window frame is shown in Fig. 17. It is shown that the stresses are increased with the window frame thickness increase. With the window frame thickness increasing, the constraint is increased, which leads to increasing in S11. And the maximum of PE22 is also increased with the increase of window frame, as shown in Fig. 18. Therefore, the thickness of window frame should not be too thick.

5.3. Effect of filler metal thickness BNi2

Keeping the rest parameters constant, the thickness of BNi2 was changed to discuss its effect on residual stress. Five FE models with a thickness of 50 μm, 75 μm, 100 μm, 125 μm and 150 μm were developed and calculated. Fig. 19 shows the effect of filler metal thickness on peak values. It can be seen that the peak stresses are decreased with the filler metal thickness increasing. Fig. 20 shows the effect of filler metal thickness on residual stresses in sealing foil, BNi2 and window frame. It presents that the stresses in the three layers are also decreased with an increase of filler metal thickness. Too thin filler metal will cause large deformation gradient in the structure, which brings difficult in stress release. When the filler metal thickness is increased, some stress could be relaxed by deformation. Therefore, the residual stresses are decreased with the filler metal thickness increase. But this does not mean that the thicker the thickness the greater the increase in strength. As mentioned in the introduction, the element boron

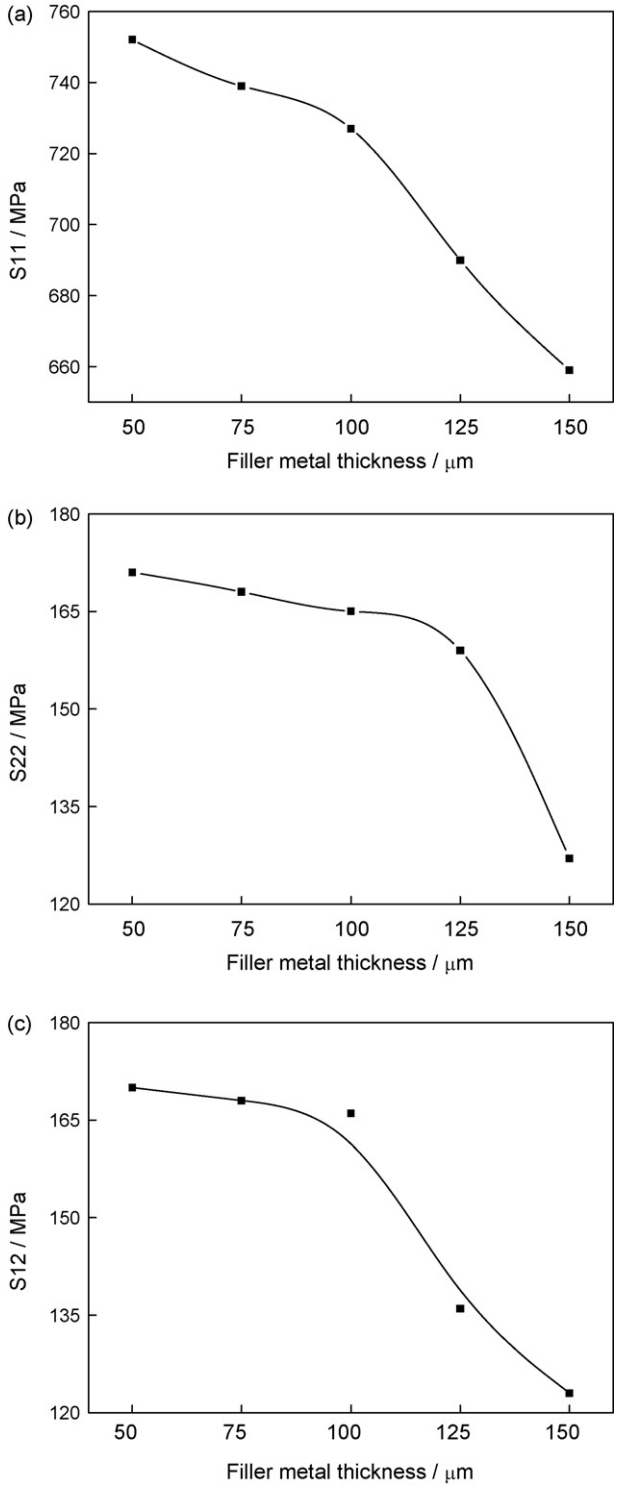

Fig. 19. Effect of filler metal thickness on peak residual stresses.

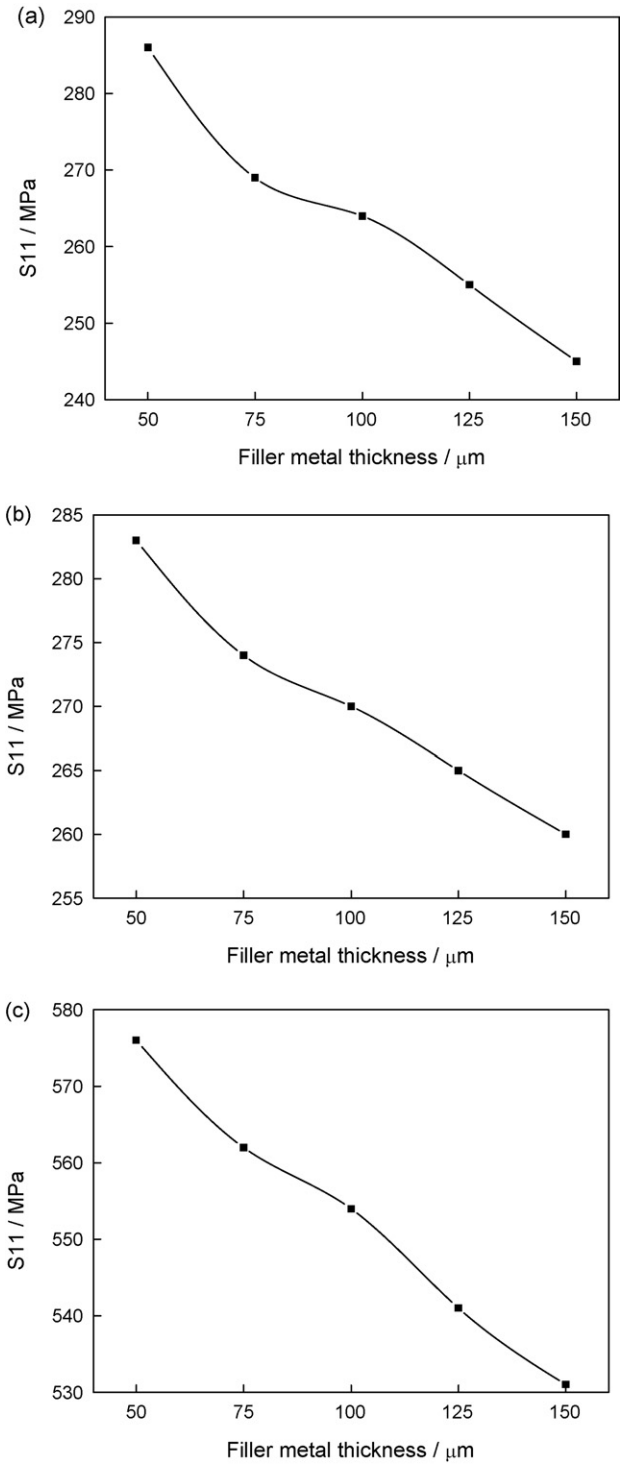

Fig. 20. Effect of filler metal thickness on S11 in sealing foil (a); BNi2 (b) and window frame (c).

is added in the filler metal BNi2. During the brazing, the boron will diffuse to sealing foil and window frame. Too thick filler metal will cause incomplete diffusion of boron. The residual boron would generate brittle phases in the brazed joint, which decreases the strength greatly. If the thickness was small enough, the boron would be fully diffused, which would help reduce the brittle phases and even form a single solid solution, thus the joint strength would be greatly enhanced. Fig. 21 shows the effect of filler metal thickness on the maximum of PE22, and their contours are not shown here to decrease the paper length. It is shown that as the filler metal thickness increases, PE22 is decreased firstly and then increased. It is very difficult to explain this phenomenon. It may be related with the whole structure features, geometric matching, strength mismatching, etc. A minimum PE22 can be obtained when a filler metal thickness of 75 μm is used, as shown in Fig. 21. Based on the considerations of stress and plastic strain, the thickness of filler metal should be determined at around 75 μm.

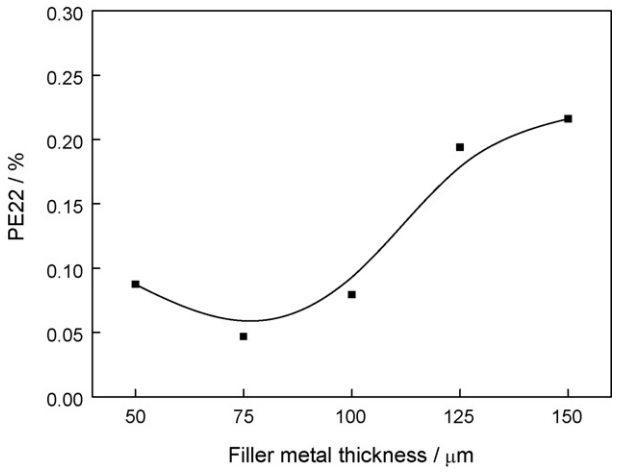

Fig. 21. Effect of filler metal thickness on the plastic strain.

6. Conclusions

This study performs a finite element analysis of as-brazed residual stress and plastic strain in the joint of sealing foil-to-window frame in BCS design of PSOFC. It is proved that the BCS design can mitigate and trap some residual stress by plastic deformation within the sealing foil. The effects of window frame material type, sealing foil thickness, filler metal thickness and window frame thickness on residual stress and plastic strain are discussed. Based on this study, the following conclusions could be achieved.

(1) Due to the mechanical properties mismatching, restraint and structure discontinuity, large residual stress are generated in the joint of sealing foil-to-window frame in BCS design. The stresses and plastic strain are concentrated in the fillet.
(2) The yield strength mismatch plays an important role on the generation of residual stress, while CTE has little effect on residual stress. With the yield strength mismatching coefficient increasing, the residual stresses are increased. Haynes 214 and Alloy 625 show a good ability to help the sealing foil to trap the plastic strain. But residual stresses generated by Alloy 625 are smaller than those obtained by Haynes 214.
(3) With the increase of sealing foil thickness, the peak stresses in the fillet are increased, while the residual stresses in sealing foil, filler metal thickness and window frame layer are decreased. The maximum plastic strain is decreased when the foil thickness is increased from 50 μm to 150 μm, but it has a sudden increase when the sealing foil is 200 μm. An optimum of sealing foil thickness is found to be 150 μm.
(4) With an increasing in the thickness of window frame, both the residual stress and the maximum plastic strain are all increased. The thickness of window frame should not be too thick.
(5) As the filler metal thickness increases, the residual stresses are decreased, while the plastic strain is firstly decreased and then increased. The optimum of filler metal thickness is found to be 75 μm.

Acknowledgments

The authors gratefully acknowledge the support provided by National Natural Science Foundation of China (No. 10472043) and Young Teachers Fund of China University of Petroleum.

References

[1] Y. Patcharavorachot, A. Arpornwichanop, A. Chuachuensuk, J. Power Sources 177 (2008) 254.
[2] M.A. Chung, J.-H. Song, I. Kang, N. Sammes, J. Power Sources 195 (2010) 821.
[3] A. Boudghene Stambouli, E. Traversa, Energy Rev. 6 (2002) 433.
[4] M.A. Priestnall, V.P. Kotzeva, D.J. Fish, E.M. Nilsson, J. Power Sources 106 (2002) 21.
[5] S.C. Singhal, Solid State Ionics 135 (2000) 305.
[6] S.C. Singhal, Solid State Ionics 152–153 (2002) 405.
[7] A. Weber, E. Ivers-Tiffée, J. Power Sources 127 (2004) 273.
[8] J.W. Fergus, J. Power Sources 147 (2005) 46.
[9] F. Smeacetto, A. Chrysanthou, M. Salvo, Z. Zhang, M. Ferraris, J. Power Sources 190 (2009) 402.
[10] K.D. Meinhardt, D.S. Kim, Y.-S. Chou, K.S. Weil, J. Power Sources 182 (2008) 188.
[11] C. Story, K. Lu, W.T. Reynolds Jr., D. Brown, Int. J. Hydrogen Energy 33 (2008) 3970.
[12] K.S. Weil, J.S. Hardy, B.J. Koeppel, J. Mater. Eng. Perform. 15 (2006) 427.
[13] K.S. Weil, B.J. Koeppel, Int. J. Hydrogen Energy 33 (2008) 3976.
[14] K.S. Weil, B.J. Koeppel, J. Power Sources 180 (2008) 343.
[15] T.L. Jiang, M.-H. Chen, Int. J. Hydrogen Energy 34 (2009) 8223.
[16] A. Joseph, S.K. Rai, T. Jayakumar, N. Murugan, Int. J. PVP 82 (2005) 700.
[17] K.S. Kim, H.J. Lee, B.S. Lee, I.C. Jung, K.S. Park, Nucl. Eng. Des. 239 (2009) 2771.
[18] C.-H. Lee, K.-H. Chang, Comput. Mater. Sci. 40 (2007) 548.
[19] W.-C. Jiang, J.-M. Gong, H. Chen, S.T. Tu, Trans. ASME J. PVT 130 (2008) 1.
[20] M. Mochizuki, Nucl. Eng. Des. 237 (2007) 107.
[21] G.F. Li, E.A. Charles, J. Congleton, Corros. Sci. 43 (2001) 1963.
[22] T. Ninh Nguyen, M.A. Wahab, J. Mater. Process. Technol. 77 (1998) 201.
[23] C.D.M. Liljedahl, J. Brouard, O. Zanellato, J. Lin, M.L. Tan, S. Gangu, et al., Int. J. Fatigue 31 (2009) 1081.
[24] X. Wu, R.S. Chandel, H. Li, H.P. Seow, S. Wu, J. Mater. Process. Technol. 1 (2000) 34.
[25] M. Pouranvari, A. Ekrami, A.H. Kokabi, J. Alloys Compd. 469 (2009) 270.
[26] M. Pouranvari, A. Ekrami, A.H. Kokab, J. Alloys Compd. 461 (2008) 641.
[27] H. Yakabe, Y. Baba, T. Sakurai, M. Satoh, I. Hirosawa, Y. Yoda, J. Power Sources 131 (2004) 278.
[28] J. Malzbender, W. Fischer, R.W. Steinbrech, J. Power Sources 182 (2008) 594.
[29] W. Fischer, J. Malzbender, G. Blass, R.W. Steinbrech, J. Power Sources 150 (2005) 73.
[30] http://www.Matweb.com.
[31] W. Jiang, J. Gong, S.T. Tu, Mater. Des. 31 (2010) 648.